

# Sequential Bayesian experimental design for estimation of extreme-event probability in stochastic dynamical systems

Xianliang Gong, Yulin Pan\*

<sup>a</sup>*Department of Naval Architecture and Marine Engineering, University of Michigan,  
48109, MI, USA*

---

## Abstract

We consider a dynamical system with two sources of uncertainties: (1) parameterized input with a known probability distribution and (2) stochastic input-to-response (ItR) function with heteroscedastic randomness. Our purpose is to efficiently quantify the extreme response probability when the ItR function is expensive to evaluate. The problem setup arises often in physics and engineering problems, with randomness in ItR coming from either intrinsic uncertainties (say, as a solution to a stochastic equation) or additional (critical) uncertainties that are not incorporated in the input parameter space. To reduce the required sampling numbers, we develop a sequential Bayesian experimental design method leveraging the variational heteroscedastic Gaussian process regression (VHGPR) to account for the stochastic ItR, along with a new criterion to select the next-best samples sequentially. The validity of our new method is first tested in two synthetic problems with the stochastic ItR functions defined artificially. Finally, we demonstrate the application of our method to an engineering problem of estimating the extreme ship motion probability in ensemble of wave groups, where the uncertainty in ItR naturally originates from the uncertain initial condition of ship motion in each wave group.

*Keywords:* extreme events, Bayesian experimental design, stochastic systems

---

\*Corresponding author  
*Email address:* yulinpan@umich.edu (Yulin Pan)

## 1. Introduction

Extreme events, considered as abnormally large response of a dynamical system, can happen in many natural and engineering systems [1, 2, 3]. Examples of such events include tsunamis, extreme precipitation and extreme structural vibrations, which often cause catastrophic consequences to the society and environment. The quantification of the probability of extreme events is of vital importance for the design of the engineering systems to alleviate their devastating impact.

Many systems of interest are characterized by an input-to-response (ItR) function which can only be queried by expensive experiments or simulations. For example, the ship motion response induced by an input wave group is obtained from expensive model of computational fluid dynamics (CFD). If the ItR function is deterministic, the probability distribution of the response is then induced only by the (assumed) known probability distribution of the input. The quantification of extreme-event probability for such systems has been studied extensively in the context of Monte-Carlo simulations. Due to the expensive evaluations of ItR and rareness of the extreme events, many studies aim for reducing the number of required samples for the computation. While techniques such as importance sampling and control variate [4] provide certain levels of acceleration, a more successful category of methods make use of the sequential Bayesian experimental design (BED) [5] (or active learning [6]), where the next-best samples are selected based on the existing information. Two key components of the sequential BED are a surrogate model (usually a Gaussian process regression [7]) to approximate the ItR, and an optimization problem maximizing a predefined acquisition function to select the next-best samples. Varying in details in the two components, a spectrum of sequential BED methods for the purpose of estimating extreme-event probability have been developed [8, 9, 10, 11, 12, 13].

However, in many cases, the ItR has to be considered as a stochastic function, instead of a deterministic one. These situations may originate from (a) an intrinsically stochastic dynamical system, e.g. stochastic differential equations modeling a physical diffusion process or stock prices [14]; the stochastic model of climate variability including the non-average ‘weather’

component as random forcing terms [15], and (b) some uncertain variables that are not easily incorporated in the input parameter space. Under such situations, the probability distribution of the response is critically influenced by the uncertainty in the ItR (in addition to the uncertainty of input parameters). Moreover, the uncertainty of the ItR (in particular the variance of response) is often inhomogeneous for different input parameters. For example, the uncertainty of power production of wind turbine is different among various wind speed inputs [16]; the uncertain ItR of ship motion resulted from uncertain initial conditions is sensitive to the wave group parameters as the input. A sequential BED method, which considers the heteroscedastic uncertainty in ItR and its effect on extreme-event probability is not yet available.

In this work, we propose a new method to quantify the probability of extreme events (defined as an observable above a given threshold) considering the ItR with heteroscedastic uncertainty. The core of our algorithm is a variational heteroscedastic Gaussian process regression (VHGPR) which approximates the ItR with sufficiently low computational cost and high accuracy. This is a critical improvement upon the standard Gaussian process regression (SGPR) used in previous work which is unable to resolve the heteroscedasticity in ItR. The VHGPR also provides significant benefits in computational cost relative to other methods such as [17], [18] and [19] where a much larger dataset are needed to resolve the ItR. Accordingly, we formulate a new acquisition function for selecting the next-best sample considering the uncertainties in both the ItR and input parameter space. We first demonstrate the effectiveness of our method in two synthetic problems to estimate the extreme-event probability. We show that drastically improved performance is achieved compared to existing approaches due to the resolution of the heteroscedasticity in ItR. Finally, we demonstrate the superiority of our method (to existing methods) in solving an engineering problem of estimating the extreme ship motion probability in irregular waves, where the ItR is established through a phenomenological nonlinear differential equations with uncertainty in its initial conditions.

## 2. Computational framework

### 2.1. Problem setup

We start from a dynamical system with input  $\mathbf{x} \in \mathbb{R}^d$  of known distribution  $X \sim p_X(\mathbf{x})$  and response  $y \in \mathbb{R}$ . An ItR function  $S$  directly relates  $\mathbf{x}$  to  $y$  with its randomness represented by  $\omega$ :

$$y(\omega) = S(\mathbf{x}, \omega), \quad \omega \in \Omega. \quad (1)$$

Our interest is the exceeding probability of  $y(\omega)$  above a threshold  $\delta$ :

$$\begin{aligned} P_e \equiv \mathbb{P}(S(X, \omega) > \delta) &= \int \mathbb{P}(S(X, \omega) > \delta | X = \mathbf{x}) p_X(\mathbf{x}) d\mathbf{x} \\ &= \int \mathbb{P}(S(\mathbf{x}, \omega) > \delta) p_X(\mathbf{x}) d\mathbf{x} \end{aligned} \quad (2)$$

It is clear that both the uncertainties associated with  $p_X$  and  $\omega$  contribute to the exceeding probability in (2). Moreover, the dependence of  $S$  on  $\mathbf{x}$  and  $\omega$ , as in (1), cannot be decoupled in general, resulting in different variance (introduced by  $\omega$ ) for different input  $\mathbf{x}$ , i.e., a heteroscedastic uncertainty. Resolving this heteroscedasticity in the ItR is critical in computing the exceeding probability (2).

A brute-force computation of (2) calls for extensive Monte-Carlo samples in the probability space associated with both  $X$  and  $\omega$  [17], which is prohibitive under expensive queries of  $S(x, \omega)$ . Therefore, we seek to develop a sampling algorithm following the sequential BED framework, where each sample is selected making use of the existing information of previous samples. Two key components in our new approach are (1) an inexpensive surrogate model based on the variational heteroscedastic Gaussian process regression (VHGPR) to approximate the heteroscedastic ItR; and (2) an optimization based on an acquisition function to provide the next-best samples with fast convergence in computing (2). We next describe the two components in detail in §2.2 and §2.3, followed by the overall algorithm 1.

### 2.2. VHGPR as a surrogate model

To introduce the surrogate model for the ItR, we first rewrite (1) as

$$S(\mathbf{x}, \omega) = f(\mathbf{x}) + R(\mathbf{x}, \omega), \quad (3)$$

where  $f(\mathbf{x}) \equiv \mathbb{E}_\omega[S(\mathbf{x}, \omega)]$  is the mean of  $S(\mathbf{x}, \omega)$  with respect to  $\omega$ , and  $R(\mathbf{x}, \omega)$  is the uncertain component with zero mean. Given a dataset (from previous samples)  $\mathcal{D} = \{\mathbf{x}^i, y^i\}_{i=1}^{i=n}$ , our purpose is to approximate (3) using Gaussian process regression as involved in many sequential BED problems.

In standard Gaussian process regression (SGPR), as implemented in most previous applications for extreme-event probability, one can approximate (3) as (given  $\mathcal{D}$ )

$$f(\mathbf{x}) \sim \mathcal{GP}(\mu_f(\mathbf{x}), \text{cov}_f(\mathbf{x}, \mathbf{x}')), \quad (4)$$

$$R(\mathbf{x}, \omega) \sim \mathcal{N}(0, \gamma_0^2), \quad (5)$$

where  $\mathcal{GP}(\cdot, \cdot)$  represents a Gaussian process with the first argument as the mean and the second as the covariance function. The uncertain component  $R(\mathbf{x}, \omega)$  is approximated by an independent normal function at all  $\mathbf{x}$  with constant variance  $\gamma_0^2$ . Clearly, the heteroscedasticity in ItR (i.e., the dependence of  $R$  on  $\mathbf{x}$ ) cannot be captured by the SGPR.

To incorporate the heteroscedasticity, we need to rely on the heteroscedastic Gaussian process regression (implemented as VHGP following [20] in this work). In VHGP, we are able to approximate (3) as (given  $\mathcal{D}$ )

$$f(\mathbf{x}) \sim \mathcal{GP}(\mu_f(\mathbf{x}), \text{cov}_f(\mathbf{x}, \mathbf{x}')), \quad (6)$$

$$R(\mathbf{x}, \omega) \sim \mathcal{N}(0, e^{g(\mathbf{x})}), \quad (7)$$

$$g(\mathbf{x}) \sim \mathcal{GP}(\mu_g(\mathbf{x}), \text{cov}_g(\mathbf{x}, \mathbf{x}')), \quad (8)$$

where the heteroscedastic (log) variance of the uncertain term  $R(\mathbf{x}, \omega)$  is represented by another  $\mathcal{GP}$  with mean  $\mu_g(\mathbf{x})$  and covariance function  $\text{cov}_g(\mathbf{x}, \mathbf{x}')$ .

Both approximations in SGPR (in terms of (4)) and VHGP ((6) and (8)) are computed as posterior predictive distributions under a Bayesian framework, with hyperparameters (say  $\boldsymbol{\theta}$ ) determined from maximizing the likelihood function  $p(\mathcal{D}|\boldsymbol{\theta})$ . For SGPR, both the likelihood function (used in training of the model) and posterior (4) can be derived analytically, allowing a straightforward and inexpensive numerical implementation. In contrast, for VHGP, the introduction of the Gaussian process on  $g(x)$  prohibits analytical results on the likelihood function and posterior, posing great chal-

lenges in the numerical computation (which involves high-dimensional integration).

In order to reduce the computational cost, variational inference is applied in VHGPR, which uses parameterized Gaussian distributions to approximate some critical distributions involved in the posterior and likelihood function. These Gaussian distributions can be determined efficiently through some optimization problem to minimize their differences from the critical distributions. As a result of this approximation, the high-dimensional integration can be reduced to analytical formulations which leads to inexpensive computations (approximations) of the posterior and the likelihood function. More details on the algorithms of the VHGPR, along with SGPR, are summarized in Appendix A for completeness. The interested readers can also refer to [7, 20] for details.

In summary, the VHGPR provides us with an estimation of the ItR,  $S(\mathbf{x}, \omega | \omega_f, \omega_g)$ , where  $\omega_f$  and  $\omega_g$  denotes realizations of  $f$  and  $g$  in (6) and (8), and  $\omega$  represents the randomness associated with (7). In other words, given realizations in  $\omega_f$  and  $\omega_g$  (or  $f$  and  $g$ ), the intrinsic randomness in ItR is expected to be captured by  $\omega$ , i.e., the heteroscedastic distribution in (7).

### 2.3. Acquisition function

Given the VHGPR of the ItR, the exceeding probability can be expressed as

$$\mathbb{P}(S(X, \omega | \omega_f, \omega_g) > \delta) = \int \mathbb{P}(S(\mathbf{x}, \omega | \omega_f, \omega_g) > \delta) p_X(\mathbf{x}) d\mathbf{x}, \quad (9)$$

which depends on the realizations in  $\omega_f$  and  $\omega_g$ . The purpose here is to construct an acquisition function, based on which the next sample can be selected to minimize the variance of the estimation (9), i.e.,  $\text{var}_{\omega_f, \omega_g}[\mathbb{P}(S(X, \omega | \omega_f, \omega_g) > \delta)]$ . For simplicity in computation, we use an upper bound of the estimation variance as its proxy (see Appendix B for the derivation of the upper bound):

$$\begin{aligned} & \text{var}_{\omega_f, \omega_g}[\mathbb{P}(S(X, \omega | \omega_f, \omega_g) > \delta)] \\ & \leq \frac{1}{2} \int \text{std}_{\omega_f, \omega_g}[\mathbb{P}(S(\mathbf{x}, \omega | \omega_f, \omega_g) > \delta)] p_X(\mathbf{x}) d\mathbf{x}, \end{aligned} \quad (10)$$

where  $\text{std}_{\omega_f, \omega_g}$  is a standard deviation operator with respect to  $\omega_f$  and  $\omega_g$ . The next-best sample is selected at the value of  $\mathbf{x}$  which contributes most to the integral on the right hand side of (10), i.e., the maximum point of the integrand corresponding to the most uncertain part in the estimation of  $\mathbb{P}(S(X, \omega | \omega_f, \omega_g) > \delta)$ :

$$\mathbf{x}^* = \operatorname{argmax}_{\mathbf{x}} \text{std}_{\omega_f, \omega_g} [\mathbb{P}(S(\mathbf{x}, \omega | \omega_f, \omega_g) > \delta)] p_X(\mathbf{x}). \quad (11)$$

We note that (11) is closely related to the so-called U criterion [10] widely used in computing the exceeding probability associated with a deterministic ItR. In general, the U criterion seeks the most ‘dangerous’ point (i.e., point with maximum local variance), which in our problem corresponds to  $\mathbf{x}^* = \operatorname{argmax}_{\mathbf{x}} \text{std}_{\omega_f, \omega_g} [\mathbb{P}(S(\mathbf{x}, \omega | \omega_f, \omega_g) > \delta)]$  (i.e., variance of (9) without considering the correlation at different  $\mathbf{x}$  and  $p_X(\mathbf{x})$ ). Therefore, our acquisition function in (11) can be considered as a weighted U criterion which incorporates the influence of the input distribution  $p_X(\mathbf{x})$  in computing the variance of (9).

In practice, we approximate the operator  $\text{std}_{\omega_f, \omega_g} \equiv (\text{var}_{\omega_f, \omega_g})^{0.5}$  by the two-dimensional spherical cubature integration [21] with 4 quadrature points (although extension to more quadrature points is straightforward):

$$m = \mathbb{E}_{\omega_f, \omega_g} [\mathbb{P}(S(\mathbf{x}, \omega | \omega_f, \omega_g) > \delta)] = \frac{1}{4} \sum_{i=1}^4 \mathbb{P}(S(\mathbf{x}, \omega | u_i)), \quad (12)$$

$$\text{var}_{\omega_f, \omega_g} [\mathbb{P}(S(\mathbf{x}, \omega | \omega_f, \omega_g) > \delta)] = \frac{1}{4} \sum_{i=1}^4 (\mathbb{P}(S(\mathbf{x}, \omega | u_i)) - m)^2, \quad (13)$$

$$\begin{aligned} u_1 &= \{f(\mathbf{x}) = \mu_f(\mathbf{x}) + \sqrt{2 \text{cov}_f(\mathbf{x})}, g(\mathbf{x}) = 0\} \\ u_2 &= \{f(\mathbf{x}) = 0, g(\mathbf{x}) = \mu_g(\mathbf{x}) + \sqrt{2 \text{cov}_g(\mathbf{x})}\} \\ u_3 &= \{f(\mathbf{x}) = -\mu_f(\mathbf{x}) - \sqrt{2 \text{cov}_f(\mathbf{x})}, g(\mathbf{x}) = 0\} \\ u_4 &= \{f(\mathbf{x}) = 0, g(\mathbf{x}) = -\mu_g(\mathbf{x}) - \sqrt{2 \text{cov}_g(\mathbf{x})}\}, \end{aligned} \quad (14)$$

where the quadrature points (14) and the corresponding weights 1/4 in (12) and (13) are selected for third-order accuracy of the scheme.

We remark that the construction of acquisition function has been studied extensively in the case of deterministic ItR [10, 9, 22, 11, 12], and that there may still be room for improvement relative to (11) in the case of uncertain ItR. These potential improvements of acquisition function may generally take consideration of correlation between different  $\mathbf{x}$  in addition to the standard deviation in (11). For example, techniques developed for deterministic ItR, such as using a hypothetical point [1, 23] and global sensitivity analysis [9], may be transferred here. However, they may lead to significantly increased computational cost when combining with VHGPR (e.g., the retraining of the variational parameters when hypothetical points are used). These potential developments will be left to our future work.

Combining the VHGPR surrogate model (Eq. (6), (7), and (8)) and the optimization of acquisition function (11), we are able to sequentially select the next-best samples starting from an initial dataset. The final estimation of exceeding probability  $P_e$  is computed by VHGPR with  $\mu_f$  and  $\mu_g$  to represent functions  $f$  and  $g$ :

$$P_e = \mathbb{P}(S(X, \omega | f(\mathbf{x}) = \mu_f(\mathbf{x}), g(\mathbf{x}) = \mu_g(\mathbf{x})) > \delta). \quad (15)$$

We summarize the algorithm of this sequential sampling process in Algorithm 1.

### 3. Results

In this section, we validate our approach using two synthetic problems and a (more) realistic engineering application to quantify the extreme ship motion probability in irregular waves. For all cases, we present the results from our current method of sequential sampling (or sequential BED) with VHGPR as a surrogate model (Seq-VHGPR), as well as other methods for validation and comparison. These other methods include Monte Carlo sampling using one million samples for accurate estimation of the mean and variance of ItR (Exact-MC, which serves as the exact result to validate Seq-VHGPR); space-filling Latin hypercube (LH) sampling [24] with VHGPR as a surrogate (LH-VHGPR, which serves as a reference to demonstrate the

---

**Algorithm 1** Sequential sampling for systems with stochastic ItR

---

**Require:** Number of initial points  $n_{init}$ , number of iterations  $n_{iter}$

**Input:** Initial dataset  $\mathcal{D} = \{\mathbf{x}^i, y^i\}_{i=1}^{i=n_{init}}$

**Initialization**  $j = 0$

**while**  $j < n_{iter}$  **do**

    Train the surrogate model (Eq. (6), (7), and (8)) with  $\mathcal{D}$

    Maximize the acquisition function (11) to find the next best sample  $\mathbf{x}^{j+1}$

    Implement numerical simulation to get  $y^{j+1} = S(\mathbf{x}^{j+1}, \omega)$

    Update the dataset  $\mathcal{D} = \mathcal{D} \cup \{\mathbf{x}^{j+1}, y^{j+1}\}$

$j = j + 1$

**end while**

**Output:** Compute the exceeding probability (15) based on the surrogate model

---

efficiency of sequential sampling); LH sampling with SGPR as a surrogate (LH-SGPR, to demonstrate the necessity of using VHGPR). We remark that the asymptotic LH-SGPR solution (with increase of sampling number) corresponds to the best solution that can be achieved by previous vast methods using SGPR [9, 10, 12, 25].

### 3.1. One-dimensional (1D) synthetic problem

We start from a 1D synthetic problem, where the true ItR  $S(x, \omega)$  (3) is constructed with (see figure 1(a) for an illustration)

$$f(x) = (x - 5)^2, \quad (16)$$

and  $R(x, \omega) \sim \mathcal{N}(0, \gamma^2(x))$  with

$$\gamma(x) = 0.1 + 0.1x^2. \quad (17)$$

The input  $X$  is assumed to follow a Gaussian distribution with  $p_X(x) = \mathcal{N}(5, 1)$ . Our objective is to estimate an exceeding probability  $P_e = \mathbb{P}(S(X, \omega) > 9)$ . For Seq-VHGPR, we use 40 LH samples as the initial data set, and show the results after 40 initial samples along with other methods.

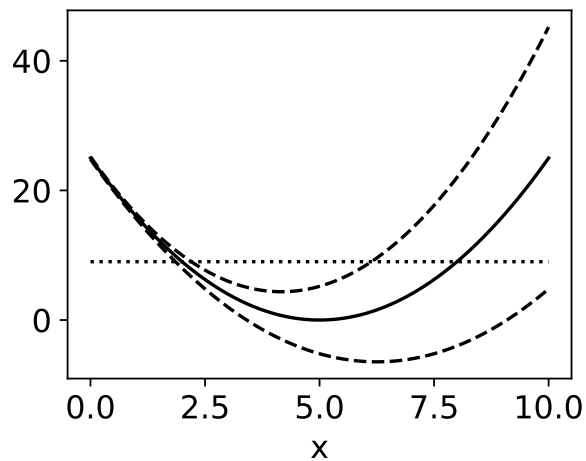


Figure 1: The mean  $f(x)$  (—) and uncertainty bounds  $f(x) \pm 2\gamma(x)$  (---) of the 1D ItR, as well as the threshold (⋯) in defining the exceeding probability.

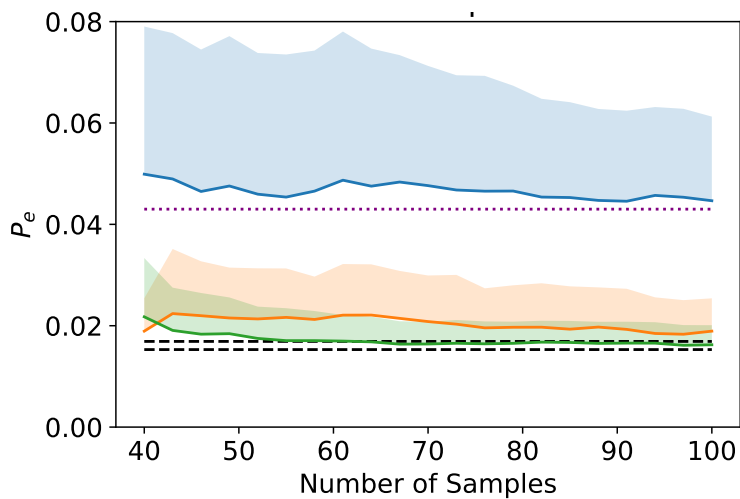


Figure 2:  $P_e$  in the 1D synthetic problem, computed by Seq-VHGPR(—), LH-VHGPR(—), LH-SGPR(—) with its asymptotic value (⋯), Exact-MC(---) (in terms of the upper and lower 5% error bounds). The shaded region represents one standard deviation above the mean estimated from 200 applications of the each method.

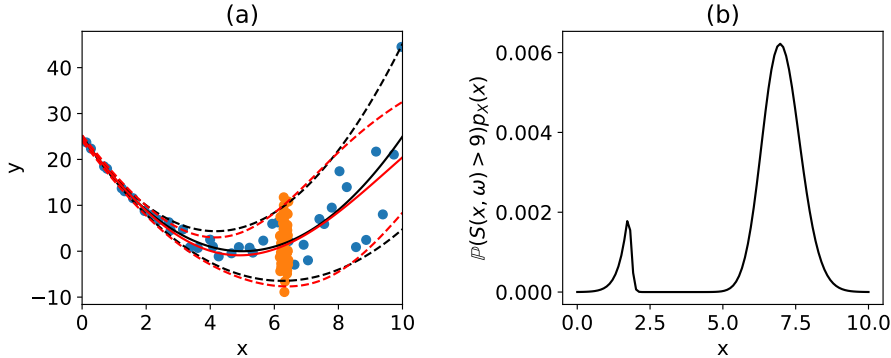


Figure 3: (a) Typical positions of initial 40 samples (●) and 60 sequential samples (●) in Seq-VHGPR, as well as the learned function  $f(x)$  (—) and  $f(x) \pm 2\gamma(x)$  (---) compared to the corresponding exact functions (—, ---); (b) the function  $\mathbb{P}(S(x, \omega) > \delta)p_X(x)$ .

Figure 2 plots the results  $P_e$  computed by Exact-MC, Seq-VHGPR, LH-VHGPR and LH-SGPR (where in Seq-VHGPR and LH-VHGPR,  $P_e$  is estimated by (15); in LH-SGPR,  $P_e$  is estimated by (15) with constant variance  $g(x) = \log(\gamma_0^2)$ ). Also included in figure 2 are the standard deviations in Seq-VHGPR, LH-VHGPR and LH-SGPR obtained from 200 applications of the methods. (These uncertainties come from the initial sampling positions and the randomness  $\omega$  of ItR in computing  $S(x, \omega)$  for each query, which is much larger than the uncertainty associated with  $f$  and  $g$  in each application.) We see that the result from Seq-VHGPR converges rapidly to that from Exact-MC (shown in terms of the 5%-error region) in the first 20 sequential samples, with an accurate estimation of the exceeding probability. In contrast, the LH-VHGPR result converges much slower, with a significant difference from the Exact-MC result at the end of 100 samples in figure 2 (in spite of a favorable trend). Furthermore, the LH-SGPR result converges to an asymptotic value which is 3 times of the Exact-MC result, showing the incapability of this class of methods (i.e., most previous methods using SGPR) in estimating the exceeding probability induced by a heteroscedastic ItR. Finally, as shown by the shaded area in figure 2, Seq-VHGPR leads to significantly reduced standard deviation compared to other approaches.

We further examine the reason for the fast convergence achieved by Seq-

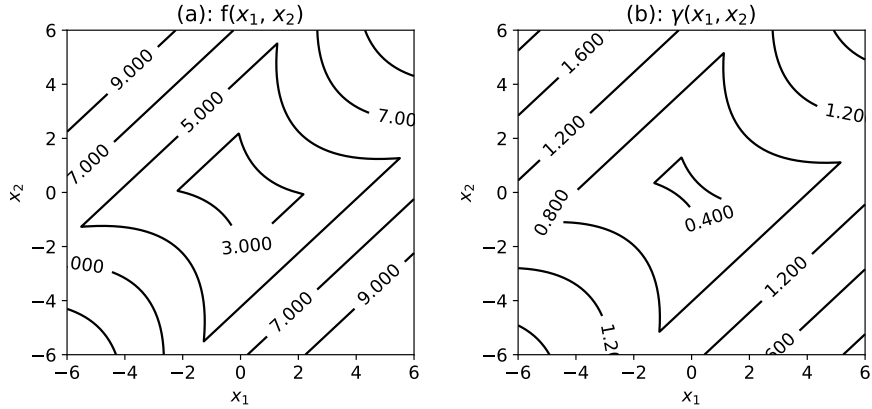


Figure 4: (a)  $f(x_1, x_2)$  and (b)  $\gamma(x_1, x_2)$  as in  $R(x_1, x_2, \omega)$  in the 2D stochastic four-branch ItR.

VHGPR (relative to LH-VHGPR). Figure 3(a) plots the positions of 100 samples (i.e., 40 initial and 60 sequential samples) in Seq-VHGPR, as well as the learned functions  $f(x)$  and  $\gamma(x)$ . While the initial 40 samples are randomly chosen (providing the overall trend of  $f(x)$  and  $\gamma(x)$ ), the 60 sequential samples are concentrated near  $x = 6.5$ , providing more accurate estimation of  $f(x)$  and  $\gamma(x)$  in the nearby region. This point corresponds to the maximum in  $\mathbb{P}(S(x, \omega) > \delta)p_X(x)$  (the integrand in (2)) as shown in figure 3(b), leading to the largest contribution in computing the exceeding probability (2).

### 3.2. Two-dimensional (2D) synthetic problem

We construct a 2D synthetic problem by setting  $f(\mathbf{x})$  to be a four-branch function (that has been widely-used in estimating extreme-event probability

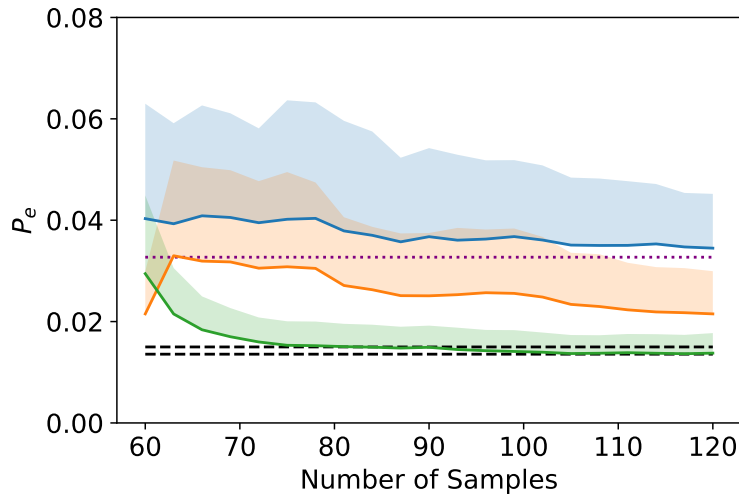


Figure 5:  $P_e$  in the 2D synthetic problem, computed by Seq-VHGPR(—), LH-VHGPR(—), LH-SGPR(—) with its asymptotic value (⋯⋯), Exact-MC(---) (in terms of the upper and lower 5% error bounds). The shaded region represents one standard deviation above the mean estimated from 200 applications of the each method.

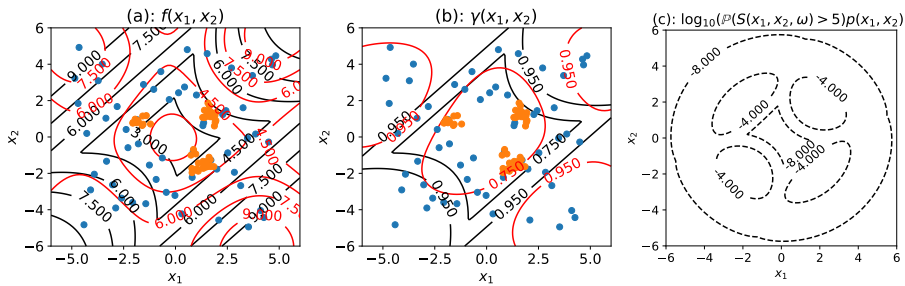


Figure 6: Typical positions of initial 60 samples (●) and 60 sequential samples (●) in Seq-VHGPR, as well as the learned  $f(x_1, x_2)$  (—) compared to the exact function (—) in (a); and the learned  $\gamma(x_1, x_2)$  (—) compared to the exact function (—) in (b); (c) the (log) function  $\mathbb{P}(S(x_1, x_2, \omega) > \delta)p_{X_1, X_2}(x_1, x_2)$ .

with a deterministic ItR) [10, 9, 25, 11]:

$$f(x_1, x_2) = -\min \begin{cases} 8 + 0.1(x_1 - x_2)^2 + \frac{(x_1 + x_2)}{\sqrt{2}} \\ 8 + 0.1(x_1 - x_2)^2 - \frac{(x_1 + x_2)}{\sqrt{2}} \\ (x_1 - x_2) + \frac{6}{\sqrt{2}} + 5 \\ (x_2 - x_1) + \frac{6}{\sqrt{2}} + 5 \end{cases}.$$

To generate an uncertain ItR, we add a Gaussian randomness  $R(x_1, x_2, \omega) \sim \mathcal{N}(0, \gamma^2(x_1, x_2))$  to  $f(x_1, x_2)$  with standard deviation  $\gamma(x_1, x_2) = f(x_1, x_2)/6$  (see figure 4 for  $f(x_1, x_2)$  and  $\gamma(x_1, x_2)$ ). We assume the input  $X$  to follow a Gaussian distribution  $p_{X_1, X_2}(x_1, x_2) = \mathcal{N}(\mathbf{0}, \mathbf{I})$ , with  $\mathbf{I}$  being a  $2 \times 2$  identity matrix, and our purpose is to estimate an exceeding probability  $P_e = \mathbb{P}(S(X_1, X_2, \omega) > 5)$ . For Seq-VHGPR, 60 LH samples are used as the initial data set.

The results of 2D problem, as shown in figure 5, further demonstrates the effectiveness of Seq-VHGPR, which approaches the Exact-MC solution with 5% error within the first 20 sequential samples and leads to the smallest uncertainty among all methods. The convergence rate of Seq-VHGPR is much faster than that of LH-VHGPR, where the latter fails to converge at the end of 120 samples. Compared with 1D results, the superiority of Seq-VHGPR over LH-VHGPR is more evident due to the increased sparsity of samples in the 2D case. The LH-SGPR result, on the other hand, converges to an asymptotic value which is 2.5 times of the Exact-MC result, a significant error due to the neglect of heteroscedastic randomness in ItR.

The typical positions of (60 initial and 60 sequential) samples in Seq-VHGPR are shown in figure 6(a)(b), as well as the learned functions  $f(x_1, x_2)$  and  $\gamma(x_1, x_2)$ . Similar to the 1D case, the sequential samples are expected to concentrate in regions where  $\mathbb{P}(S(x_1, x_2, \omega) > \delta)p_{X_1, X_2}(x_1, x_2)$  is maximized, i.e., the four regions enclosed by -4 contour lines in figure 6(c). As shown in figure 6(a)(b), most sequential samples lie in three out of the four regions (although the situation depends on the initial samples and for some cases all four regions can be filled). The difficulty of the sequential

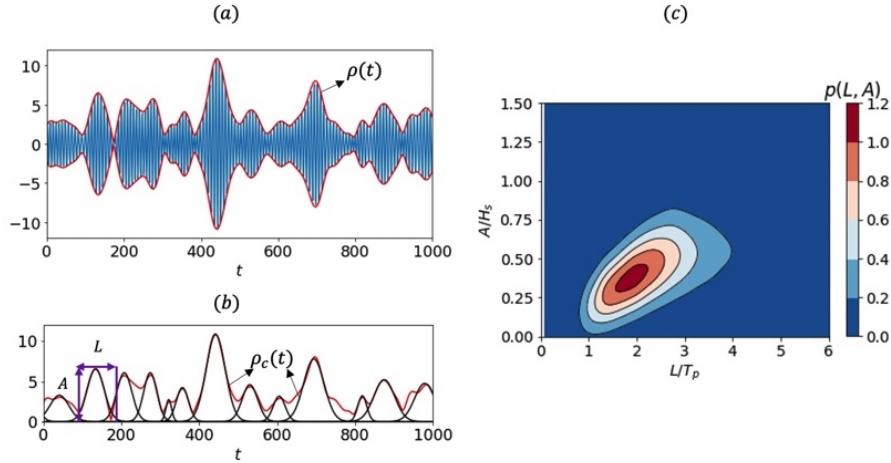


Figure 7: (a)  $\eta(t)$  (—) and the corresponding  $\rho(t)$  (—) in a narrow-band wave field. (b)  $\rho(t)$  (—) fitted by an ensemble of Gaussian wave groups  $\rho_c(t)$ (—) with parameters  $L$  and  $A$ . (c)  $p_{L,A}(L, A)$  obtained from wave fields.

samples transiting to all four regions within 60 samples can be anticipated, which is consistent with the observation in the case of deterministic ItR if the U criterion is used as the acquisition function [10]. While the design of better acquisition function is possible referring to the counterpart in the deterministic case [9], the current results already show the adequacy of Seq-VHGPR in estimating the exceeding probability (even if not all four regions are filled and the estimation of  $\gamma(x_1, x_2)$  is relatively less accurate than that of  $f(x_1, x_2)$ ).

### 3.3. Probability of extreme ship motion in irregular waves

We further consider an engineering application of our method to estimate the probability of extreme ship roll motions in uni-directional irregular waves. In marine engineering, the ship motion problem can often be treated as a dynamical system where the input is a time series of wave (or surface) elevation  $\eta(t)$ , and the output is, say, the ship roll motion  $\xi(t)$ . The ItR connecting  $\eta(t)$  and  $\xi(t)$  can be computed by Computational Fluid Dynamics (CFD) simulations. However, the resolution of exact exceeding probability requires running expensive CFD simulations with a very long-

time input  $\eta(t)$  (due to the rareness of the extreme roll motion), leading to prohibitively high computational cost. Therefore, for the purpose of validating our approach, we use an inexpensive phenomenological nonlinear roll equation [26] to construct the ItR (with the uncertainty associated with  $\omega$  introduced later)

$$\ddot{\xi} + \alpha_1 \dot{\xi} + \alpha_2 \xi^3 + (\beta_1 + \epsilon_1 \cos(\phi)\eta(t))\xi + \beta_2 \xi^3 = \epsilon_2 \sin(\phi)\eta(t), \quad (18)$$

with empirical coefficients [27]  $\alpha_1 = 0.19$ ,  $\alpha_2 = 0.06$ ,  $\beta_1 = 0.04$ ,  $\beta_2 = -0.1$ ,  $\epsilon_1 = 0.020$ ,  $\epsilon_2 = 0.004$ , and  $\phi = \pi/6$ .

The wave elevation  $\eta(t)$  is usually specified from a wave spectral process, which resides in a high-dimensional input space. A typical procedure to reduce the dimension is to describe  $\eta(t)$  by an ensemble of wave groups embedded in its envelope process [28, 1] (see figure 7(a) for an illustration, which is only strictly valid in narrow-band wave spectrum). Specifically, we compute the envelope process  $\rho(t)$  from  $\eta(t)$  through the Hilbert transform [29], and then construct two-parameter Gaussian-like wave groups  $\rho_c(x)$  which best fits  $\rho(t)$ :

$$\rho_c(t) \sim A \exp \frac{-(t - t_c)^2}{2L^2}, \quad (19)$$

where  $t_c$  is the temporal location of the group, and the two parameters  $A$  (group amplitude) and  $L$  (group length) describe the geometry of the group (figure 7(b)). This dimension-reduction procedure allows  $\eta(t)$  to be described by an ensemble of  $(L, A)$  wave groups, i.e., a two-dimensional input parameter space (see figure 7(c)). We can then construct an ItR with the input as  $(L, A)$  to (18) and the output as the maximum roll through this wave group, and consider the group-based probability.

However, sampling in the  $(L, A)$  space (with each sample as the input to (18) with pre-defined initial condition, say  $\xi(0) = 0$  and  $\dot{\xi}(0) = 0$  as in [8, 30]) loses critical information associated with  $\eta(t)$ . The most important one among them is the varying initial condition of the ship at the encounter of each wave group. As shown in [31, 32], (18) (and the ship roll in general) may be sensitive to the initial conditions for some  $A$  and  $L$  (see figure 8 as

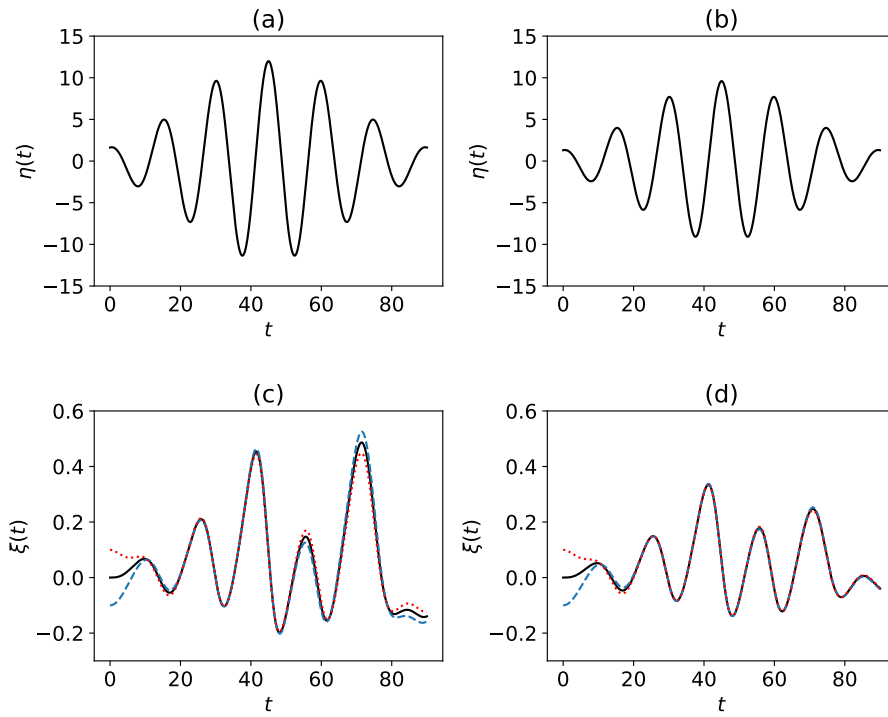


Figure 8: The roll responses (c) and (d) with different initial conditions  $\{\dot{\xi}(0) = 0, \xi(0) = 0\}$  (—);  $\{\dot{\xi}(0) = 0, \xi(0) = -0.05\}$  (- - -);  $\{\dot{\xi}(0) = 0, \xi(0) = 0.05\}$  (· · · · ·), computed from (18) with input from a wave group with respectively (a) larger and (b) smaller amplitudes.

an example). This creates heteroscedastic uncertainty in the ItR (associated with  $\omega$ ) that needs to be dealt with by our current approach Seq-VHGPR.

In the following, we show the results with input  $\eta(t)$  extracted from a narrow-band Gaussian wave spectrum:

$$F(k) = \frac{H_s^2}{16} \frac{1}{\sqrt{2\pi}\mathcal{K}} \exp \frac{-(k - k_0)^2}{2\mathcal{K}^2}, \quad (20)$$

with significant wave height  $H_s = 12m$ , peak (carrier) wavenumber  $k_0 = 0.018m^{-1}$  (corresponding to peak period  $T_p = 15s$ ), and  $\mathcal{K} = 0.05k_0$ . The exact exceeding probability is computed by simulating 1500 hours (36000  $T_p$ ) of ship responses. To compute the ItR incorporating the heteroscedastic randomness in  $\omega$ , after a sample  $(L, A)$  is chosen, we randomly select a wave group of this  $(L, A)$  in  $\rho(x)$ , and simulate (18) starting from (on average) 5 groups ahead of the  $(L, A)$  group with a  $(0, 0)$  initial condition. Since the impact of initial conditions typically decay in  $O(1)$  wave group, we are able to naturally capture the true initial condition as the ship encounters the  $(L, A)$  group.

Figure 9 plots  $P_e = \mathbb{P}(\max(\xi_{L,A}(t)) > 0.3)$  (the probability that maximum roll in a group exceeds 17 degrees) obtained from Seq-VHGPR, LH-VHGPR, LH-SGPR and the exact solution. We see that the Seq-VHGPR result converges to the exact solution within the first 30 sequential samples, much faster than the convergence of the LH-VHGPR result. The LH-SGPR result converges to an asymptotic value which is appreciably larger than the exact solution. We remark that this value represents the best result that can be achieved by all previous methods on this problem [8, 30] based on SGPR. These results, again, demonstrate the effectiveness of Seq-VHGPR in computing the exceeding probability relative to all other approaches.

#### 4. Conclusions

In this paper, we present a new method (Seq-VHGPR) to efficiently estimate the extreme-event probability (in terms of the exceeding probability) induced by an ItR with heteroscedastic uncertainty. The method is established in the framework of sequential BED, and leverages the VHGPR as a

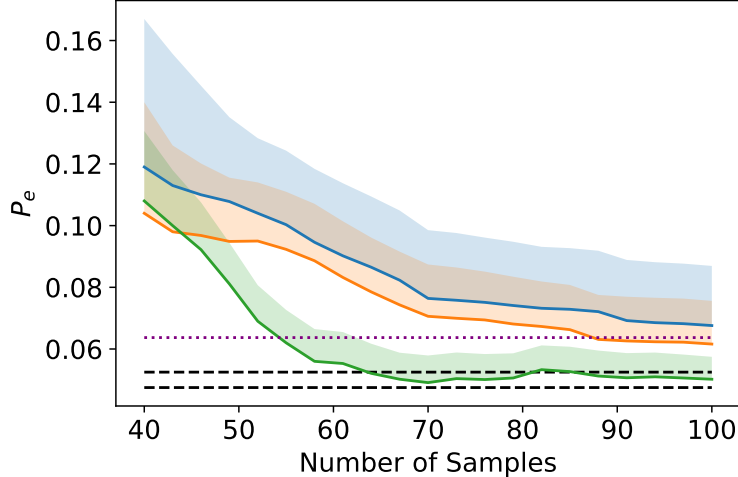


Figure 9:  $P_e$  in the ship roll problem, computed by Seq-VHGPR(—), LH-VHGPR(—), LH-SGPR(—) with its asymptotic value (⋯⋯), exact solution(---) (in terms of the upper and lower 5% error bounds). The shaded region represents one standard deviation above the mean estimated from 200 applications of the each method.

surrogate model to estimate the uncertain ItR. A new acquisition function corresponding to the VHGPR estimation is developed to select the next-best sequential sample which leads to fast convergence of the exceeding probability. We validate our new method in two synthetic problems and one engineering application to estimate the extreme ship motion probability in irregular waves. In all cases, we find fast convergence of Seq-VHGPR to the exact solution, demonstrating its superiority to all existing methods if an ItR with heteroscedastic uncertainty is associated with the problem. This is indeed due to the effectiveness of VHGPR in estimating the ItR, although there is still room for improvement of the acquisition function to accelerate the convergence as done in the case of deterministic ItR [9]. Finally, we remark that the present method also provides a potential way for high-dimensional BED, where the most influential dimensions can be selected as (low-dimensional) input  $X$ , with other secondary ones packaged into  $\Omega$  in the ItR (as in the ship motion problem).

## ACKNOWLEDGEMENT

This research is supported by the Office of Naval Research grant N00014-20-1-2096. We thank the program manager Dr. Woei-Min Lin for several helpful discussions on the research.

## References

- [1] M. Farazmand, T. P. Sapsis, Extreme events: Mechanisms and prediction, *Applied Mechanics Reviews* 71 (5) (2019).
- [2] M. Ghil, P. Yiou, S. Hallegatte, B. Malamud, P. Naveau, A. Soloviev, P. Friederichs, V. Keilis-Borok, D. Kondrashov, V. Kossobokov, et al., Extreme events: dynamics, statistics and prediction, *Nonlinear Processes in Geophysics* 18 (3) (2011) 295–350.
- [3] S. Rahmstorf, D. Coumou, Increase of extreme events in a warming world, *Proceedings of the National Academy of Sciences* 108 (44) (2011) 17905–17909.
- [4] A. B. Owen, *Monte Carlo theory, methods and examples*, 2013.
- [5] K. Chaloner, I. Verdinelli, Bayesian experimental design: A review, *Statistical Science* (1995) 273–304.
- [6] D. A. Cohn, Z. Ghahramani, M. I. Jordan, Active learning with statistical models, *Journal of artificial intelligence research* 4 (1996) 129–145.
- [7] C. E. Rasmussen, *Gaussian processes in machine learning*, in: *Summer School on Machine Learning*, Springer, 2003, pp. 63–71.
- [8] M. A. Mohamad, T. P. Sapsis, Sequential sampling strategy for extreme event statistics in nonlinear dynamical systems, *Proceedings of the National Academy of Sciences* 115 (44) (2018) 11138–11143.
- [9] Z. Hu, S. Mahadevan, Global sensitivity analysis-enhanced surrogate (gsas) modeling for reliability analysis, *Structural and Multidisciplinary Optimization* 53 (3) (2016) 501–521.

- [10] B. Echard, N. Gayton, M. Lemaire, Ak-mcs: an active learning reliability method combining kriging and monte carlo simulation, *Structural Safety* 33 (2) (2011) 145–154.
- [11] H. Wang, G. Lin, J. Li, Gaussian process surrogates for failure detection: A bayesian experimental design approach, *Journal of Computational Physics* 313 (2016) 247–259.
- [12] B. J. Bichon, M. S. Eldred, L. P. Swiler, S. Mahadevan, J. M. McFarland, Efficient global reliability analysis for nonlinear implicit performance functions, *AIAA journal* 46 (10) (2008) 2459–2468.
- [13] A. Blanchard, T. Sapsis, Output-weighted optimal sampling for bayesian experimental design and uncertainty quantification, *arXiv e-prints* (2020) arXiv–2006.
- [14] H. Holden, B. Øksendal, J. Ubøe, T. Zhang, Stochastic partial differential equations, in: *Stochastic partial differential equations*, Springer, 1996, pp. 141–191.
- [15] K. Hasselmann, Stochastic climate models part i. theory, *tellus* 28 (6) (1976) 473–485.
- [16] T. Rogers, P. Gardner, N. Dervilis, K. Worden, A. Maguire, E. Papatheou, E. Cross, Probabilistic modelling of wind turbine power curves with application of heteroscedastic gaussian process regression, *Renewable Energy* 148 (2020) 1124–1136.
- [17] P. Perdikaris, D. Venturi, J. O. Royset, G. E. Karniadakis, Multi-fidelity modelling via recursive co-kriging and gaussian–markov random fields, *Proceedings of the Royal Society A: Mathematical, Physical and Engineering Sciences* 471 (2179) (2015) 20150018.
- [18] L. Le Gratiet, Multi-fidelity gaussian process regression for computer experiments, Ph.D. thesis (2013).

- [19] L. Parussini, D. Venturi, P. Perdikaris, G. E. Karniadakis, Multi-fidelity gaussian process regression for prediction of random fields, *Journal of Computational Physics* 336 (2017) 36–50.
- [20] M. Lázaro-Gredilla, M. K. Titsias, Variational heteroscedastic gaussian process regression, in: *ICML*, 2011.
- [21] E. A. Wan, R. Van Der Merwe, The unscented kalman filter for non-linear estimation, in: *Proceedings of the IEEE 2000 Adaptive Systems for Signal Processing, Communications, and Control Symposium (Cat. No. 00EX373)*, Ieee, 2000, pp. 153–158.
- [22] Z. Zhu, X. Du, Reliability analysis with monte carlo simulation and dependent kriging predictions, *Journal of Mechanical Design* 138 (12) (2016).
- [23] P. Pandita, I. Bilonis, J. Panchal, Bayesian optimal design of experiments for inferring the statistical expectation of expensive black-box functions, *Journal of Mechanical Design* 141 (10) (2019).
- [24] M. D. McKay, R. J. Beckman, W. J. Conover, A comparison of three methods for selecting values of input variables in the analysis of output from a computer code, *Technometrics* 42 (1) (2000) 55–61.
- [25] Z. Sun, J. Wang, R. Li, C. Tong, Lif: A new kriging based learning function and its application to structural reliability analysis, *Reliability Engineering & System Safety* 157 (2017) 152–165.
- [26] N. Umeda, H. Hashimoto, D. Vassalos, S. Urano, K. Okou, Nonlinear dynamics on parametric roll resonance with realistic numerical modelling, *International shipbuilding progress* 51 (2, 3) (2004) 205–220.
- [27] A. H. Nayfeh, D. T. Mook, P. Holmes, *Nonlinear oscillations* (1980).
- [28] M. S. Longuet-Higgins, On the joint distribution of wave periods and amplitudes in a random wave field, *Proceedings of the Royal Society of London. A. Mathematical and Physical Sciences* 389 (1797) (1983) 241–258.

- [29] K. Shum, W. K. Melville, Estimates of the joint statistics of amplitudes and periods of ocean waves using an integral transform technique, *Journal of Geophysical Research: Oceans* 89 (C4) (1984) 6467–6476.
- [30] X. Gong, Z. Zhang, K. Maki, Y. Pan, Full resolution of extreme ship response statistics, *33rd Symposium on Naval Hydrodynamics* (2000).
- [31] P. A. Anastopoulos, K. J. Spyrou, Evaluation of the critical wave groups method in calculating the probability of ship capsize in beam seas, *Ocean Engineering* 187 (2019) 106213.
- [32] M. S. Soliman, J. Thompson, Transient and steady state analysis of capsize phenomena, *Applied Ocean Research* 13 (2) (1991) 82–92.
- [33] C. M. Bishop, *Pattern recognition and machine learning*, springer, 2006.
- [34] S. Kullback, R. A. Leibler, On information and sufficiency, *The annals of mathematical statistics* 22 (1) (1951) 79–86.

## Appendix A. Algorithms for Gaussian Process Regression

We consider the task of inferring the input to response (ItR) function from a dataset  $\mathcal{D} = \{\mathbf{x}^i, y^i\}_{i=1}^{i=n}$  consisting of  $n$  inputs  $\mathbb{X} = \{\mathbf{x}^i \in \mathbb{R}^d\}_{i=1}^{i=n}$  and the corresponding outputs  $\mathbf{y} = \{y^i \in \mathbb{R}\}_{i=1}^{i=n}$ .

### Appendix A.1. Standard Gaussian Process Regression (SGPR)

SGPR assumes the function to be a sum of a mean  $f(\mathbf{x})$  and a Gaussian randomness with constant variance  $\gamma_0^2$  (at all  $\mathbf{x}$ ):

$$y = f(\mathbf{x}) + R \quad R \sim \mathcal{N}(0, \gamma_0^2), \quad (\text{A.1})$$

A prior, representing our beliefs over all possible functions we expect to observe, is placed on  $f$  as a Gaussian process  $f(\mathbf{x}) \sim \mathcal{GP}(0, k_f(\mathbf{x}, \mathbf{x}'))$  with zero mean and covariance function  $k_f$  (usually defined by a radial-basis-function kernel):

$$k_f(\mathbf{x}, \mathbf{x}') = \tau^2 \exp\left(-\frac{1}{2} \sum_{j=1}^{j=d} \frac{(x_j - x'_j)^2}{l_j^2}\right), \quad (\text{A.2})$$

where the amplitude  $\tau^2$  and length scales  $l_j$ , together with  $\gamma_0$ , are hyperparameters  $\boldsymbol{\theta} = \{\tau, l_j, \gamma_0\}$  in SGPR.

Following the Bayesian formula, the posterior prediction for  $f$  given the dataset  $\mathcal{D}$  can be derived to be another Gaussian:

$$p(f(\mathbf{x})|\mathcal{D}) = \frac{p(f(\mathbf{x}), \mathbf{y})}{p(\mathbf{y})} = \mathcal{N}(\mu_f(\mathbf{x}), \text{cov}_f(\mathbf{x})), \quad (\text{A.3})$$

with analytically tractable mean  $\mu_f(\mathbf{x})$  and covariance  $\text{cov}_f(\mathbf{x}, \mathbf{x}')$ :

$$\mu_f(\mathbf{x}) = k_f(\mathbf{x}, \mathbb{X})^T (\mathbf{K}_f(\mathbb{X}, \mathbb{X}) + \gamma_0^2 \mathbf{I})^{-1} \mathbf{y}, \quad (\text{A.4})$$

$$\text{cov}_f(\mathbf{x}, \mathbf{x}') = k_f(\mathbf{x}, \mathbf{x}') - k_f(\mathbf{x}, \mathbb{X})^T (\mathbf{K}_f(\mathbb{X}, \mathbb{X}) + \gamma_0^2 \mathbf{I})^{-1} k_f(\mathbf{x}', \mathbb{X}), \quad (\text{A.5})$$

where matrix element  $\mathbf{K}_f(\mathbb{X}, \mathbb{X})_{ij} = k_f(\mathbf{x}^i, \mathbf{x}^j)$ . The hyperparameters  $\boldsymbol{\theta}$  are determined which maximizes the likelihood function  $p(\mathcal{D}|\boldsymbol{\theta}) \equiv p(\mathbf{y}|\boldsymbol{\theta}) = \mathcal{N}(0, \mathbf{K}_f(\mathbb{X}, \mathbb{X}) + \gamma_0^2 \mathbf{I})$ .

#### *Appendix A.2. Variational Heteroscedastic Gaussian Process Regression (VHGPR)*

In this section, we briefly outline the algorithm of VHGPR. The purpose is to provide the reader enough information to understand the logic behind VHGPR. For the conciseness of the presentation, some details in the algorithm have to be omitted. We recommend the interested readers to read [20] and §10 in [33] for details.

In VHGPR, the function of ItR is considered as the sum of a mean and a Gaussian term (independent at all  $\mathbf{x}$ ) with heteroscedastic uncertainty:

$$y = f(\mathbf{x}) + R \quad R \sim \mathcal{N}(0, e^{g(\mathbf{x})}). \quad (\text{A.6})$$

Two Gaussian priors are placed on the mean and the (log) variance function:

$$f(\mathbf{x}) \sim \mathcal{GP}(0, k_f(\mathbf{x}, \mathbf{x}')), \quad (\text{A.7})$$

$$g(\mathbf{x}) \sim \mathcal{GP}(\mu_0, k_g(\mathbf{x}, \mathbf{x}')), \quad (\text{A.8})$$

where  $k_f$  and  $k_g$  are respectively the radial-basis-function kernels for  $f$  and  $g$ , defined similarly as (A.2).  $\mu_0$  is the prior mean for  $g$ . The hyperparameters in VHGPR can then be defined as  $\boldsymbol{\theta} = (\mu_0, \boldsymbol{\theta}_f, \boldsymbol{\theta}_g)$  where  $\boldsymbol{\theta}_{f,g}$  includes the

amplitudes and length scales involved in  $k_f$  or  $k_g$ . Moreover, we assume  $f$  is independent with  $g$ .

The increased expressive power with the heteroscedastic variance is at the cost of analytically intractable likelihood (for determination of hyper-parameters) and posterior (prediction). Let  $\mathbf{f} = f(\mathbb{X})$  and  $\mathbf{g} = g(\mathbb{X})$  denote the realizations of mean and variance at training inputs  $\mathbb{X}$  following the distributions in (A.7) and (A.8). The likelihood and prediction are formulated as:

$$p(\mathcal{D}|\boldsymbol{\theta}) \equiv p(\mathbf{y}|\boldsymbol{\theta}) = \iint p(\mathbf{y}|\mathbf{f}, \mathbf{g})p(\mathbf{g}|\boldsymbol{\theta})p(\mathbf{f}|\boldsymbol{\theta})d\mathbf{g}d\mathbf{f}, \quad (\text{A.9})$$

$$p(f(\mathbf{x}), g(\mathbf{x})|\mathcal{D}) = \iint p(f(\mathbf{x}), g(\mathbf{x})|\mathbf{f}, \mathbf{g})p(\mathbf{f}, \mathbf{g}|\mathbf{y})d\mathbf{f}d\mathbf{g}. \quad (\text{A.10})$$

Since analytical integration cannot be achieved for (A.9) and (A.10), numerical evaluations of the integrals are needed for their computations. However, the dimension of integration (w.r.t  $\mathbf{f}$  and  $\mathbf{g}$ ) is the same as number of data points  $n$ , which can be prohibitively high for a direct integration, say, using quadrature methods. While the Monte-Carlo method (e.g., MCMC) offers some advantages in computational cost, its application is still too expensive for most practical problems. For these problems, the VHGPB leveraging variational inference is the only method which provides practical solutions with low computational cost and sufficient accuracy.

The key distribution in computing (A.10) and (A.9) is  $p(\mathbf{f}, \mathbf{g}|\mathbf{y})$  (directly involved in (A.10) and related to (A.9) due to (A.11) that will be discussed), which is however expensive to compute directly. The key idea in VHGPB is to approximate  $p(\mathbf{f}, \mathbf{g}|\mathbf{y})$  by  $q(\mathbf{f}, \mathbf{g})$ , where the latter is assumed to have a Gaussian distribution with parameters (multi-dimensional means and covariance) denoted here by  $\boldsymbol{\theta}_q$ . Through minimizing the KL divergence [34] between  $p(\mathbf{f}, \mathbf{g}|\mathbf{y})$  and  $q(\mathbf{f}, \mathbf{g})$ , the parameters  $\boldsymbol{\theta}_q$  can be determined and both the posterior and likelihood can be evaluated accordingly as discussed below.

For the posterior, (A.10) becomes a linear Gaussian model (an integration of the exponential of quadratic function of  $\mathbf{f}$  and  $\mathbf{g}$  with Gaussian weights) which has an analytical formulation. For the likelihood, we avoid

directly using (A.9) but decompose  $\log p(\mathbf{y}|\boldsymbol{\theta})$  as a summation of the evidence lower bound (ELBO)  $\mathcal{L}(q(\mathbf{f}, \mathbf{g}))$  and the K-L divergence between  $q(\mathbf{f}, \mathbf{g})$  and  $p(\mathbf{f}, \mathbf{g}|\mathbf{y})$ <sup>1</sup>:

$$\log p(\mathbf{y}|\boldsymbol{\theta}) = \mathcal{L}(q(\mathbf{f}, \mathbf{g})) + \text{KL}(q(\mathbf{f}, \mathbf{g})|p(\mathbf{f}, \mathbf{g}|\mathbf{y})), \quad (\text{A.11})$$

where

$$\mathcal{L}(q(\mathbf{f}, \mathbf{g})) = \iint q(\mathbf{f}, \mathbf{g}) \log \frac{p(\mathbf{y}, \mathbf{f}, \mathbf{g})}{q(\mathbf{f}, \mathbf{g})} d\mathbf{f}d\mathbf{g}, \quad (\text{A.12})$$

$$\text{KL}(q(\mathbf{f}, \mathbf{g})|p(\mathbf{f}, \mathbf{g}|\mathbf{y})) = \iint q(\mathbf{f}, \mathbf{g}) \log \frac{q(\mathbf{f}, \mathbf{g})}{p(\mathbf{f}, \mathbf{g}|\mathbf{y})} d\mathbf{f}d\mathbf{g}. \quad (\text{A.13})$$

We then formulate an optimization problem of  $\mathcal{L}$  (where  $\mathcal{L}$ , as a weighted integration of the exponential function of  $\mathbf{f}$  and  $\mathbf{g}$ , has an analytical expression for Gaussian weights  $q(\mathbf{f}, \mathbf{g})$  [33]) to determine both the parameters in  $q(\mathbf{f}, \mathbf{g})$  ( $\boldsymbol{\theta}_q$ ) and the hyperparameters ( $\boldsymbol{\theta}$ ):

$$\boldsymbol{\theta}_q^*, \boldsymbol{\theta}^* = \operatorname{argmax}_{\boldsymbol{\theta}_q, \boldsymbol{\theta}} \mathcal{L}(\boldsymbol{\theta}_q, \boldsymbol{\theta}). \quad (\text{A.14})$$

We remark that (A.14) can be conceived as two sequential optimization problems with respect to  $\boldsymbol{\theta}_q$  and  $\boldsymbol{\theta}$ . For the former, maximizing  $\mathcal{L}$  is equivalent to minimizing the KL divergence (as an aforementioned goal) since  $\log p(\mathbf{y}|\boldsymbol{\theta})$  in (A.11) is not a function of  $\boldsymbol{\theta}_q$ . For the latter, since the KL divergence has been minimized, the ELBO gives a good approximation of likelihood  $\log p(\mathbf{y}|\boldsymbol{\theta})$ . Therefore, the solution of (A.14) simultaneously provides the optimal  $\boldsymbol{\theta}_q$  leading to a good approximation of  $p(\mathbf{f}, \mathbf{g}|\mathbf{y})$  by  $q(\mathbf{f}, \mathbf{g})$ , as well as the optimal  $\boldsymbol{\theta}$  leading to a maximized likelihood.

However, (A.14) with respect to  $\boldsymbol{\theta}_q$  is still a prohibitively expensive optimization with dimensions  $2n + 2n(2n + 1)/2$  (i.e., number of unique elements in the mean and co-variance matrix of  $q(\mathbf{f}, \mathbf{g})$ ). To reduce the number of dimensions, a key procedure employed in VHGPR is to assume that the

---

<sup>1</sup>This decomposition can be derived from manipulation of (A.13) to be

$$\text{KL}(q(\mathbf{f}, \mathbf{g})|p(\mathbf{f}, \mathbf{g}|\mathbf{y})) = - \iint q(\mathbf{f}, \mathbf{g}) \log \frac{p(\mathbf{y}, \mathbf{f}, \mathbf{g})}{q(\mathbf{f}, \mathbf{g})} d\mathbf{f}d\mathbf{g} + \log p(\mathbf{y}).$$

function  $q(\mathbf{f}, \mathbf{g})$  is separable in  $\mathbf{f}$  and  $\mathbf{g}$ , i.e.,  $q(\mathbf{f}, \mathbf{g}) = q_f(\mathbf{f})q_g(\mathbf{g})$ . This brings two benefits: First, one can show that the maximized solution of  $\mathcal{L}$  involves a relation between  $q_f(\mathbf{f})$  and  $q_g(\mathbf{g})$ , i.e.,  $q_f(\mathbf{f})$  can be represented as a function of  $q_g(\mathbf{g})$  so that the parameters in  $\boldsymbol{\theta}_q$  is reduced to the mean  $\boldsymbol{\mu}$  and covariance  $\Sigma$  of  $q_g(\mathbf{g})$  (with dimension  $n + n(n + 1)/2$ ). Second, the stationary point of  $\mathcal{L}$  with respect to  $\boldsymbol{\mu}$  and  $\Sigma$  (by making  $\partial\mathcal{L}/\partial\boldsymbol{\mu} = \mathbf{0}$  and  $\partial\mathcal{L}/\partial\Sigma = \mathbf{0}$ ) leads to an analytical form

$$\boldsymbol{\mu} = \mathbf{K}_g(\mathbb{X}, \mathbb{X})(\Lambda - \frac{1}{2}\mathbf{I})\mathbf{1} + \mu_0\mathbf{1}, \quad (\text{A.15})$$

$$\Sigma = (\mathbf{K}_g(\mathbb{X}, \mathbb{X})^{-1} + \Lambda)^{-1}, \quad (\text{A.16})$$

with  $\mathbf{K}_g(\mathbb{X}, \mathbb{X})_{ij} = k_g(\mathbf{x}^i, \mathbf{x}^j)$ ,  $\Lambda$  being a diagonal matrix involving  $n$  unknown parameters and  $\mathbf{1}$  being a vector with all elements 1. Therefore the optimization (A.14) is finally reduced to

$$\Lambda^*, \boldsymbol{\theta}^* = \operatorname{argmax}_{\Lambda, \boldsymbol{\theta}} \mathcal{L}(\boldsymbol{\mu}(\Lambda), \Sigma(\Lambda), \boldsymbol{\theta}), \quad (\text{A.17})$$

with only  $n$  parameters in  $\boldsymbol{\theta}_q$  (or  $\Lambda$ ). This can be solved by gradient-based method, with the major computational cost in computing  $n \times n$  matrix inversions in  $\mathcal{L}$ . The computational cost of each iteration in (A.17) is only approximately twice as that in SGPR.

With  $q_f(\mathbf{f})$ ,  $q_g(\mathbf{g})$  (computed from  $\Lambda^*$ ), and  $\boldsymbol{\theta}$  available, the posterior predictions for  $f$  and  $g$  in (A.10) are:

$$\begin{aligned} p(f(\mathbf{x}), g(\mathbf{x})|\mathcal{D}) &= \iint p(f(\mathbf{x}), g(\mathbf{x})|\mathbf{f}, \mathbf{g})q_f(\mathbf{f})q_g(\mathbf{g})d\mathbf{f}d\mathbf{g} \\ &= \iint p(f(\mathbf{x})|\mathbf{f})p(g(\mathbf{x})|\mathbf{g})q_f(\mathbf{f})q_g(\mathbf{g})d\mathbf{f}d\mathbf{g} \\ &\quad (\text{independence of } f(\mathbf{x}) \text{ and } g(\mathbf{x})) \\ &= \int p(f(\mathbf{x})|\mathbf{f})q_f(\mathbf{f})d\mathbf{f} \int p(g(\mathbf{x})|\mathbf{g})q_g(\mathbf{g})d\mathbf{g} \\ &= p(f(\mathbf{x})|\mathcal{D})p(g(\mathbf{x})|\mathcal{D}), \end{aligned} \quad (\text{A.18})$$

where:

$$p(f(\mathbf{x})|\mathcal{D}) = \mathcal{N}(\mu_f(\mathbf{x}), \text{cov}_f(\mathbf{x}, \mathbf{x}')), \quad (\text{A.19})$$

$$p(g(\mathbf{x})|\mathcal{D}) = \mathcal{N}(\mu_g(\mathbf{x}), \text{cov}_g(\mathbf{x}, \mathbf{x}')), \quad (\text{A.20})$$

$$\mu_f(\mathbf{x}) = k_f(\mathbf{x}, \mathbb{X})^T (\mathbf{K}_f(\mathbb{X}, \mathbb{X}) + Z)^{-1} \mathbf{y}, \quad (\text{A.21})$$

$$\text{cov}_f(\mathbf{x}, \mathbf{x}') = k_f(\mathbf{x}, \mathbf{x}') - k_f(\mathbf{x}, \mathbb{X})^T (\mathbf{K}_f(\mathbb{X}, \mathbb{X}) + Z)^{-1} k_f(\mathbf{x}', \mathbb{X}), \quad (\text{A.22})$$

$$\mu_g(\mathbf{x}) = k_g(\mathbf{x}, \mathbb{X})^T (\Lambda - \frac{1}{2}\mathbf{I})\mathbf{1} + \mu_0, \quad (\text{A.23})$$

$$\text{cov}_g(\mathbf{x}, \mathbf{x}') = k_g(\mathbf{x}, \mathbf{x}') - k_g(\mathbf{x}, \mathbb{X})^T (\mathbf{K}_g(\mathbb{X}, \mathbb{X}) + \Lambda^{-1})^{-1} k_g(\mathbf{x}', \mathbb{X}), \quad (\text{A.24})$$

with  $Z_{ii} = e^{\mu_i - \Sigma_{ii}/2}$  being a diagonal matrix and  $\mathbf{K}_f(\mathbb{X}, \mathbb{X})_{ij} = k_f(\mathbf{x}^i, \mathbf{x}^j)$ .

## Appendix B. The upper bound of the estimation variance

Here we show the construction of an upper bound of the estimation variance (For convenience we use  $\hat{p}_\omega(\mathbf{x})$  to represent  $\mathbb{P}(S(\mathbf{x}, \omega | \omega_f, \omega_g) > \delta)$ ):

$$\begin{aligned} & \text{var}_{\omega_f, \omega_g} [\mathbb{P}(S(X, \omega | \omega_f, \omega_g) > \delta)] \\ &= \text{var}_{\omega_f, \omega_g} \left[ \int \hat{p}_\omega(\mathbf{x}) p_X(\mathbf{x}) d\mathbf{x} \right] \\ &= \mathbb{E}_{\omega_f, \omega_g} \left[ \left( \int \hat{p}_\omega(\mathbf{x}) p_X(\mathbf{x}) d\mathbf{x} \right)^2 \right] - \left( \mathbb{E}_{\omega_f, \omega_g} \left[ \int \hat{p}_\omega(\mathbf{x}) p_X(\mathbf{x}) d\mathbf{x} \right] \right)^2 \\ &= \mathbb{E}_{\omega_f, \omega_g} \left[ \int \hat{p}_\omega(\mathbf{x}) p_X(\mathbf{x}) d\mathbf{x} \int \hat{p}_\omega(\mathbf{x}') p_X(\mathbf{x}') d\mathbf{x}' \right] \\ &\quad - \left( \mathbb{E}_{\omega_f, \omega_g} \left[ \int \hat{p}_\omega(\mathbf{x}) p_X(\mathbf{x}) d\mathbf{x} \right] \right) \left( \mathbb{E}_{\omega_f, \omega_g} \left[ \int \hat{p}_\omega(\mathbf{x}') p_X(\mathbf{x}') d\mathbf{x}' \right] \right) \\ &= \iint \mathbb{E}_{\omega_f, \omega_g} \left[ \hat{p}_\omega(\mathbf{x}) \hat{p}_\omega(\mathbf{x}') \right] p_X(\mathbf{x}) p_X(\mathbf{x}') d\mathbf{x} d\mathbf{x}' \\ &\quad - \int \int \mathbb{E}_{\omega_f, \omega_g} \left[ \hat{p}_\omega(\mathbf{x}) \right] \mathbb{E}_{\omega_f, \omega_g} \left[ \hat{p}_\omega(\mathbf{x}') \right] p_X(\mathbf{x}) p_X(\mathbf{x}') d\mathbf{x} d\mathbf{x}' \\ &= \iint \text{cov}_{\omega_f, \omega_g} \left[ \hat{p}_\omega(\mathbf{x}), \hat{p}_\omega(\mathbf{x}') \right] p_X(\mathbf{x}) p_X(\mathbf{x}') d\mathbf{x} d\mathbf{x}' \\ &= \int \text{std}_{\omega_f, \omega_g} \left[ \hat{p}_\omega(\mathbf{x}) \right] \left( \int \text{std}_{\omega_f, \omega_g} \left[ \hat{p}_\omega(\mathbf{x}') \right] \rho_{\omega_f, \omega_g} \left[ \hat{p}_\omega(\mathbf{x}), \hat{p}_\omega(\mathbf{x}') \right] p_X(\mathbf{x}') d\mathbf{x}' \right) p_X(\mathbf{x}) d\mathbf{x} \\ &\leq 0.5 \int \text{std}_{\omega_f, \omega_g} \left[ \hat{p}_\omega(\mathbf{x}) \right] p_X(\mathbf{x}) d\mathbf{x} \end{aligned} \quad (\text{B.1})$$

where  $\rho[\cdot, \cdot]$  denotes the correlation coefficient. The last inequality comes from  $\text{std}_{\omega_f, \omega_g}[\hat{p}_\omega(\mathbf{x}')] \leq 0.5$  and  $\rho_{\omega_f, \omega_g}[\hat{p}_\omega(\mathbf{x}), \hat{p}_\omega(\mathbf{x}')] \leq 1$ . The equality in (B.1) holds when  $\hat{p}_\omega$  degenerates to a Bernoulli random variable with equal probability 0.5 at both  $\hat{p}_\omega = 0$  and  $\hat{p}_\omega = 1$  and  $\rho_{\omega_f, \omega_g}[\hat{p}_\omega(\mathbf{x}), \hat{p}_\omega(\mathbf{x}')] = 1$ .